Validating the rhenium proxy for rock organic carbon oxidation using weathering profiles

Katherine E. Grant, Mathieu Dellinger, Alexander J. Dickson, Mateja Ogric, Kate Horan, Steve Petsch, Robert G. Hilton

Validating the rhenium proxy for rock organic carbon oxidation using weathering profiles

Katherine E. Grant[1,2]*, Mathieu Dellinger[2,3], Alexander J. Dickson[4], Mateja Ogric[2], Kate Horan[2], Steve Petsch[5], Robert G. Hilton[6]*

1. Center for Accelerator Mass Spectrometry, Lawrence Livermore National Laboratory, Livermore, CA 94550, USA
2. Department of Geography, Department of Earth Sciences, Durham University, Durham, DH1 3LE, UK
3. Environnements Dynamiques et Territoires de la Montagne (EDYTEM), CNRS – Université Savoie Mont-Blanc, Le Bourget du Lac, 73370, France
4. Centre of Climate, Ocean and Atmosphere, Department of Earth Sciences, Royal Holloway University of London, Egham, Surrey, TW20 0EX, UK
5. Department of Earth, Geographic, and Climate Sciences, University of Massachusetts, Amherst, MA 01003, USA
6. Department of Earth Sciences, University of Oxford, South Parks Rd, Oxford, OX1 3AN, UK

*corresponding authors; grant39@llnl.gov; robert.hilton@earth.ox.ac.uk

Abstract

Chemical weathering over geological timescales acts as a source or sink of atmospheric carbon dioxide (CO_2), while influencing long-term redox cycling and atmospheric oxygen (O_2) at Earth's surface. There is a growing recognition that the oxidative weathering of rock organic carbon (OC_{petro}) can release more CO_2 than is locally drawn down by silicate weathering, and may vary due to changes in erosion and climate. The element rhenium (Re) has emerged as a proxy to track the oxidative weathering of OC_{petro}, yet uncertainties in its application remain namely that we lack a systematic assessment of the comparative mobility of Re and OC_{petro}

during sedimentary rock weathering. Here we measure Re and OC_{petro} loss across gradients in rock weathering at 12 global sites, spanning a range of initial OC_{petro} values from ~0.2% to >10%. At nine sites we use titanium to account for volume changes during weathering and assess Re and OC_{petro} loss alongside major elements that reflect silicate (Na, Mg), carbonate (Ca, Mg) and sulfide (S) weathering. Across the dataset, Re loss is correlated with OC_{petro} loss but not with loss of any other major element. Across the weathering profiles, the average molar ratio of OC_{petro} to Re loss was 0.84 ± 0.15, with 8 out of 9 sites having a ratio >0.74. At one site (Marcellus Shale), the average ratio was lower at 0.58 ± 0.11. The excess loss of Re matches expectations that, typically, between ~0–20% of the Re liberated by sedimentary rock weathering derives from silicate or sulfide phases, while some OC_{petro} may be physically or chemically protected from weathering. Overall, our measurements provide validation for the Re proxy of OC_{petro} oxidation and allow future work to further improve our knowledge of regional and global-scale rates of this important source of CO_2 in the geochemical carbon cycle.

1. Introduction:

When sedimentary rocks are brought to Earth's surface during exhumation and erosion (Blair et al., 2003; Hilton et al., 2011), organic matter that is millions of years old re-enters the contemporary carbon cycle (Copard et al., 2007; Petsch, 2014; Petsch et al., 2000; Wildman et al., 2004). The oxidative weathering of this rock-derived organic carbon (petrogenic OC; OC_{petro}) can release carbon dioxide (CO_2) and consume oxygen (O_2) (Petsch, 2014; Roylands et al., 2024; Soulet et al., 2021) at globally significant rates (Zondervan et al., 2023). In addition, the importance of physical erosion in driving weathering fluxes (Bolton et al., 2006; Hilton et al., 2014) raises the question as to whether oxidative weathering has changed alongside global denudation (Syvitski et al., 2005) through the Cenozoic (Salles et al., 2023). To move forward,

49 we require measurements of oxidative weathering across scales, which will allow us to build and
50 test quantitative models that explore its role in setting long-term CO_2 and O_2 concentrations
51 (Berner, 2003; Zondervan et al., 2023) and, assess how weathering and erosion combine to force
52 net exchanges of carbon between the lithosphere and atmosphere (Hilton and West, 2020).

53 Rhenium (Re) is a proxy that can track and quantify oxidative weathering of rock organic
54 carbon. Re and organic matter are coupled during shallow marine diagenesis as marine sediment
55 porewaters become anoxic (Colodner et al., 1993; Crusius and Thomson, 2000) and Re is
56 immobilized. A close association of Re and OC_{petro} in sedimentary rocks has been recognized
57 (Selby and Creaser, 2003). The first studies of Re mobility during weathering revealed a coupled
58 loss of Re and OC_{petro} in a black shale weathering profile (Jaffe et al., 2002; Peucker-Ehrenbrink
59 and Hannigan, 2000). Upon oxidation, Re is soluble as perrhenate (ReO_4^-) and is thought to be
60 carried away from the reaction site by water (Colodner et al., 1993), while the carbon may be
61 released as CO_2 (Keller and Bacon, 1998; Soulet et al., 2018) or mobilized as dissolved organic
62 carbon (Schillawski and Petsch, 2008). Following the work of Dalai et al., (2002), a growing
63 number of studies have used the dissolved Re flux (or oxidized Re flux) from a landscape to
64 estimate oxidative weathering of OC_{petro} (Ghazi et al., 2022; Hilton et al., 2014; Hilton et al.,
65 2021; Horan et al., 2019; Horan et al., 2017). The oxidative weathering flux (or yield) of OC_{petro},
66 $J_{OCpetro\text{-}ox}$ (tC yr^{-1}), is usually calculated from the measured dissolved rhenium flux (J_{Re}) (t yr^{-1})
67 (Dalai et al., 2002; Dellinger et al., 2023; Hilton et al., 2014), using:

68 $$J_{OCpetro-ox} = J_{Re} \times \left(\frac{[OC_{petro}]}{[Re]}\right)_i \times f_c \times (1 - f_{graphite}) \quad (1)$$

69 where $([OC_{petro}]/[Re])_i$ is the initial concentration ratio in the rocks undergoing weathering. The
70 term f_C is the fraction of the dissolved Re flux derived from OC_{petro}, with the remainder
71 mobilized by weathering other phases, e.g. sulfide and silicate minerals (Horan et al., 2019). The

final term $f_{graphite}$ recognizes a fraction of the OC_{petro} pool which may not be susceptible to oxidation, for instance in high grade metamorphic rocks where graphite is present (Galy et al., 2008; Horan et al., 2017). In addition, some landscapes with low weathering rates and local historic fossil fuel burning power plants or other industries may have contributions of Re to river waters (Ogrič et al., 2023).

To validate the Re proxy for OC_{petro} oxidation and reduce the uncertainty in its application (Zondervan et al., 2023), we need to quantify coupled loss of Re and OC_{petro} over a range of possible weathering environments. Although Re measurements have become more common (Sheen et al., 2018), especially in river environments (Dellinger et al., 2021; Hilton et al., 2014; Horan et al., 2017; Ogrič et al., 2023), we still lack comprehensive tests of Re loss from the solid phase residue of weathering (Jaffe et al., 2002; Ogrič et al., 2023); especially in weathering profiles ranging in OC content, sulfur content and reactive Fe content (Petsch et al., 2000). Measuring the residual weathered material can give site-specific insights into what products are release during weathering. The Re proxy can be applied to river fluxes (Equation 1), but can also be calculated from solid samples if landscape weathering profiles are available. In terms of the residual phases of weathering (e.g. soils) that can be found in the landscape, OC_{petro} oxidation can be constrained as:

$$J_{OCpetro-ox} = -D \times (\left[OC_{petro}\right]_{w*} - \left[OC_{petro}\right]_{i*}) \quad (2)$$

$$J_{Re} = -D \times ([Re]_{w*} - [Re]_{i*}) \quad (3)$$

where D is the total denudation rate (t yr^{-1}), the subscript w refers to the concentration in the products of weathering in the landscape compared to the initial, *i*, and * refers to a correction for concentration changes associated with volume changes with weathering as both increases in volume due to plant and organic matter deposition and mass loss associated with chemical

weathering and volumetric strain need to be accounted for (Brimhall and Dietrich, 1987; Chadwick et al., 1990; Hayes et al., 2019). From this, Equation 1 can be re-written as:

$$\frac{([OC_{petro}]_w - [OC_{petro}]_i)}{[OC_{petro}]_i} = \frac{([Re]_w - [Re]_i)}{[Re]_i} \times f_c \times (1 - f_{graphite}) \quad (4)$$

which demonstrates how, if the Re proxy was operating to track OC_{petro}, weathering products should show coupled loss of OC_{petro} and Re, moderated by the factors f_C and $f_{graphite}$.

Here we address how well Re can trace OC_{petro} during rock weathering through new analysis of previously collected and freshly sampled weathering profiles across 9 sites and combine these data with previously published studies to create a compiled data set of 104 measurements. These include samples from weathered and unweathered black shales (OC > 1 wt. %) and organic rich mudstones which we term here "grey shales" (OC < 1 wt.%) which are globally relevant to Re and OC_{petro} weathering fluxes (Sheen et al., 2018; Zondervan et al., 2023). Re mobility is assessed alongside OC_{petro}, using radiocarbon (^{14}C) where appropriate, and major and trace elements to track silicate, carbonate, and sulfide mineral weathering. We use the index element titanium (Ti) at the 9 sites to account for pedogenic volume changes (Kurtz et al., 2000) and calculate a "loss ratio" to understand the coupled loss of OC_{petro} and Re across different systems and evaluate the use of the Re proxy.

2. Materials and Methods:

Table 2. List of tectonic and climate information for the sampling sites.

Location	Rock type	Tectonic Setting	Relief	Climate[1]
Waiapoa	gray shale	active	High	Temperate
Waipu	gray shale	active	High	Temperate
Marcellus	black shale	inactive	modest	humid continental
New Albany (Clay city)	black shale	inactive	modest	humid continental

Woodford Shale	black shale	inactive	modest	humid tropical
Green River	black shale	inactive	modest	Steppe
Monterey	black shale	active	High	Mediterranean
Taiwan	grey shale	active	High	Sub-tropical Rainforest
East River	grey shale	inactive	High	Steppe

[1]Based on zones reported in Beck et al., 2023

2.1 Weathering profiles

New measurements were made on 40 individual samples which included a set of six black shale weathering profiles (n =33) (OC_{petro} > 1%) collected from across the continental USA, and two grey shale weathering profiles (n= 7) (OC_{petro} < 1%) collected from New Zealand. Black shale samples were processed to analyze Re and major elements from profiles characterized previously for OC_{petro}, and S loss (Petsch, 2014; Petsch et al., 2000). The samples include the six sites published in Petsch et al. (2000) and additionally reviewed in Petsch (2014). Briefly, at each site we have 4–6 samples ranging from highly weathered to un-weathered from collected from road cuts. To reduce possibility for interbed variability, collected samples were carefully chosen to sample single sedimentary beds or horizons (Table 1).

The six collection sites are listed with their geologic age and measured %OC content in the un-weathered samples (Petsch et al., 2000), they range across different erosional settings from teconically inactive to active, while covering three different climatic zones. The New Albany Shale (Clay City; NACC) and New Albany Shale (Deatsville; NADV) are of late Devonian Age, and have un-weathered OC contents ranging between 9–12% OC. The NACC samples were collected from Clay City, Powell Co., Kentucky, USA and the NADV samples were collected from Deatsville, Nelson Co., Kentucky, USA. The Woodford shale (WF) is also Devonian in age, with a variable 15–25% OC in the un-weathered samples. These were collected

from Arbuckle Mtns., Murray Co., Oklahoma, USA. The Marcellus shale (ME) is mid-Devonian age and samples collected contain 8–10% OC in the un-weathered shale. These samples are from Warren, Herkimer Co., New York, USA. The Monterey shale (MO) is Miocene age and collected from Gaviota Beach, Santa Barbara Co., California, USA. The OC contents range from 8–20% in the un-weathered samples. The Green River shale (GR) is from the Eocene and was collected from Nine Mile Canyon, Duchesne Co., Utah, USA; unweathered samples contain 15–18% OC.

The mid to late Devonian shales (NACC, NADV, WF, and ME) were all deposited in oxygen-deficient, highly productive epeiric seas on the craton of eastern North America (Petsch et al., 2000). The New Albany and ME shales contain abundant clay and detrital quartz, whereas the WF is more silica rich. These organic sediments are mainly composed of marine phytoplankton with minor contributions from bacteria and terrestrial plants. These rocks have abundant pyrite formation and limited OM sulfurization. The GR, an Eocene formation, is a lacustrine formation formed by the rise of the Rocky Mountains and is dominated by carbonate-rich marl. There is low sulfate and detrital iron which limited OM sulfurization and pyrite formation. The Miocene MO formation was deposited in a restricted marine basin off the Californian coast. It is composed of siliceous sediments with marine carbonates and some detrital material derived from the Coastal Range mountains. These organic matter rich rocks are low in pyrite and had high OM sulfurization leading to large sulfur rich organic macromolecules. The OM is mainly marine phytoplankton and bacteria with some terrestrial plant material. There are three main types of OM from this study (I, II, and II-S), where GR is Type I, NACC, NADV, WF, and ME are Type II, and MO is Type II-S. All of these rocks, except for ME, are thermally

156 immature and are expected to have a lower degree of graphitization than thermally mature
157 shales.

158 Two sites in New Zealand that were sampled represent lower OC_{petro} contents more
159 typical of the majority of continental surface rocks (Zondervan et al., 2023). These are from the
160 Waipaoa (WPO) catchment, collected in April 2018 and the Waiapu (WPU) catchment collected
161 in September 2014. Both weathering profiles were collected from road cuts, with samples of
162 weathered material near the modern vegetation and soil interface, and less weathered material
163 with depth in the profile. In this part of New Zealand, the Raukumara Ranges (Kuehl et al.,
164 2016) experience ongoing tectonic uplift and high rates of denudation which expose a sequence
165 of deformed but weakly metamorphosed Cretaceous and Tertiary sedimentary rocks, dominated
166 by mudstones (Mazengarb and I.G.Speden, 2000). The WPO profile is located on the mid
167 Miocene Tolaga Group, and is comprised of grey, slightly calcareous mudstones. The WPU
168 profile formed on the same geological unit but is located to the northern part of the Raukumara
169 peninsular, where mudstones with minor carbonate content are interbedded with fine sandstones.
170 The Early Cretaceous mudstones of the Mokoiwi Formation (Ruatoria Group) which outcrop to
171 the north of this location have been the focus of a field-based study of CO_2 production during
172 mudstone weathering (Roylands et al., 2022) and have OC_{petro} contents of ~0.7–0.8 %.
173

174 **2.2 Published data**

175 Three profiles with previously published rhenium concentration and OC data are used in this
176 study. In those works, OC_{petro} concentration was determined using radiocarbon activity and a two
177 end member mixing model to account for biospheric contribution to the OC (Zhang et al, 2024).
178 We include samples from the Upper Devonian Ohio Shale (Jaffe et al., 2002), the East River

Bradley Meadow site (Hilton et al., 2021), and samples from the Central Range in Taiwan (Hilton et al., 2014; Hilton et al., 2010). The Ohio Shale is the same shale as the previously described NACC black shale. It was sampled by Petsch and others from the same roadcut from Clay City, Kentucky in 2009, but from a distinct sedimentary horizon. Re and OC_{petro} concentrations were previously reported in Jaffe et al. (2002), and Re isotopic composition was reported in (Miller et al., 2015). The East River Bradley Meadow site is instrumented within the Lawrence Berkely National Laboratory's Watershed Function Scientific Focus Area (SFA) (Winnick et al., 2017) and is located in the upper East River catchment of the Colorado Rocky Mountains. The soil-subsurface profile was collected in 2019 and is a subalpine meadow located at 2,987 m elevation. [Re], TOC and $F^{14}C$ data were first presented in Hilton et al. (2021). Paired [Re] and OC_{petro} loss was also calculated in solid samples from the Central Range Taiwan, where weathered materials from soils (Hemingway et al., 2018) were compared to less weathered OC_{petro} in riverbed materials (Hilton et al., 2014). The Taiwan case provides a higher metamorphic grade case study than most of the other sites. All samples utilized in this study are presented in Table 1 and 2.

2.3 Geochemical methods

Carbon isotopic measurements

The majority of samples used in this study had previously reported organic carbon concentrations, organic carbon isotope composition (stable isotopes, radiocarbon), and OC_{petro} concentrations. The Waipaoa and Waiapu profiles were analyzed and reported here for the first time. The black shale samples used in this study were previously measured for OC concentration ([OC],%), stable isotope composition ($\delta^{13}C$; ‰),^{14}C ($F^{14}C$, "fraction modern") and pyrite sulfur

([S],%) determined by H_2S liberation with acidic $CrCl_2$ and reported in Petsch et al. (2001b) and Petsch et al. (2000). For a subset of the grey shale samples, Taiwan and East River, we use previously reported carbon isotopic measurements and OC_{petro} concentrations (Hilton et al., 2014; Hilton et al., 2021). The Waiapu grey shale samples were measured for [OC], $\delta^{13}C$, and ^{14}C after a 0.2 N HCl leaching protocol (Galy et al., 2007) to remove carbonates following Horan et al., (2017). Aliquots of dried sample were loaded into pre-combusted tin capsules for EA-IRMS measurement at Durham University. Samples were measured on a Costech elemental analyzer coupled to a Thermo Fisher Scientific V Advantage Isotope Ratio Mass spectrometer and normalized to the composition of international standards (reported relative to Vienna Pee Dee Belemnite with a precision of 0.2‰). The Waiapu WPU grey shale profile samples were analyzed for the radiocarbon activity (reported as Fraction Modern, $F^{14}C$) at the University of California, Irvine Keck Carbon Cycle Facility following closed tubed combustion and graphitization (Horan et al., 2017). The Waipaoa WPO grey shale was processed using the HCl fumigation method to remove carbonates (Komada, et al., 2008), while the radiocarbon activity (reported as $F^{14}C$) was measured o at ETH-Zurich at the Laboratory of Ion Beam Physics using the coupled EA-Mini Radiocarbon Dating System (MICADS) with CO_2 as the source of the ion beam. (McIntyre et al., 2017). Each radiocarbon faculty uses standard background corrections and reports data according to Stuiver and Polach (1977). $F^{14}C$ measurements were used to constrain a two-endmember mixing model to calculate an OC_{petro} concentration for the Waipaoa and Waiapu profiles, with a $F^{14}C$ value for OC_{petro} of 0, and the biospheric end member having a $F^{14}C = 1.0 \pm 0.1$ which reflects the steep, shallow organic soils in these setting.

Sample handling and digestion

For the new Re data reported here, the black shale samples and WPO profile were ground to a fine powder in an agate planetary rotary mill and then digested with modified methods reported by Dellinger et al. (2020). Due to a concurrent aim to obtain enough Re mass for isotopic measurements (not reported here), larger masses for the black shale samples were used than are strictly necessary for [Re] measurements. Briefly, sample aliquots (~500 mg) were loaded into Savilex Teflon beakers and digested with 2:1 16 M HNO3: 10 M HCl aqua regia solution for 24 hours. Samples were dried down at 80 ºC and digested with ~1–3 ml 29 M HF to remove silica content, then slowly dried again at 80 ºC before being redigested at 120 ºC in aqua regia to remove precipitated fluorides. This process was repeated ~3 times to ensure complete digestion.

For the black shales, after an initial, extended digestion, the high refractory OC content of the black shales lead to a black solid residue. A set of 30 ml BaekDu^{TM} Digestion Vessels from ODLAB were used to rapidly digest the organic matter content of these samples, with the principal benefit of these vessels being a continued, repeated reflux of the sample through deliberate and focused formation of an acid reflux that slightly pressurized and concentrated the digestion residue. The sample was weighed into the bottom of the vessel with 3ml 16 M HNO_3 then the interior cap was placed on the beaker and the exterior cap was filled with 2ml 16 M HNO_3, to ensure constant, sustained reflux. The reactor vessels were then heated on a hotplate overnight (~12–16 hrs) at 200 ºC. The entire sample (liquid and solid) was then transferred to a Savillex Teflon beaker and silicates were removed through the HF digestion procedure described above. These reactor vessels cut the entire digestion time to ~24–36 hours from the previous 2–4 weeks. Digested samples were redissolved in 1 M HCl and a sample aliquot which we ensured was <1% of total [Re] was taken for trace metal concentration analysis.

To purify for the black shale and WPO profile sample for [Re] measurement, the sample, with 1% total volume for total elemental analysis, was loaded onto a preconditioned polypropylene column with 1 ml AG1-X8 (200–400ml) resin according to methods described in Dellinger et al. (2020). The sample was washed with 10 ml 1 M HNO_3, 15ml 0.5 HNO_3, 1.5ml 4M HNO_3, and then Re was eluted in 4 M HNO_3 and dried down. Samples were refluxed with 16 M HNO_3 at 150ºC to remove any column bleed and diluted to an appropriate range to measure [Re].

The WPU profile was digested using similar methods as described above, but was analyzed using isotope dilution ICP-MS and purified using a solvent extraction. In summary, ~0.05 g of sediment sample was doped with a known amount of ^{185}Re solution and digested in a 6:3 concentrated HF-HNO_3 mix (9 mL) for 24 hours at 120 °C, evaporated, then digested again in a 2:1 mix of concentrated HNO_3-HCl (3 mL) for 24 h at 120 °C. The Re was isolated from the matrix using a NaOH-acetone solvent extraction (Cumming et al., 2013; Horan et al., 2019).

Major elements and Trace elements

Major and trace elements were analyzed on an ICP-OES at Durham University after dilution to appropriate concentration ranges. A set of 6 to 7 multi-element calibration standards with concentrations ranging from 0.1 to 60 ppm were used. USGS shale rock standards MAG-1 (n=2 digestions and measurements), SDO-1 (n=1) and SBC-1 (n=2) were measured to assess the precision and accuracy of the measurements. Data agree with USGS certified values to within <5% for Al_2O_3, <7% for Fe_2O_3, <8% for CaO, <9% for MgO, <10% for TiO_2, and <20% for Na_2O, K_2O and MnO.

Rhenium measurements

All Re measurements, apart from those on the WPU profile, were made by multi-collector inductively coupled plasma mass spectrometry (MC-ICP-MS; ThermoFisher Scientific NeptunePlus without jet interface) at the Arthur Holmes Isotope Geology Laboratory, Dept. Earth Sciences, University of Durham. Following separation of Re, samples were re-dissolved in 0.5 M HNO_3 and a small aliquot (~2% of the sample mass) was taken to measure Re concentration by MC-ICP-MS. External calibration curves were determined via sample dilution (Dellinger et al., 2020).

The WPU profile was analyzed from purified Re aliquots in 0.8 M HNO_3 using a Thermo Scientific X-Series Q-ICP-MS to analyze the modified Re isotope composition (following ^{185}Re spike addition) and corrected for mass fractionation and blank contributions (Horan et al., 2019). Concentrations were calculated by isotope dilution using the measured $^{185}Re/^{187}Re$ ratio. The sample precision and accuracy of these methods and those used in the literature previously (Dellinger et al., 2021; Hilton et al., 2014; Jaffe et al., 2002) are not vastly different, and we do not expect any systematic biases between the specific analysis protocols used.

2.4 Metric of loss

To accurately quantify the loss of an element of interest, in this case, Re or OC_{petro}, normalization to an immobile, 'index', element is a common practice (Brimhall and Dietrich, 1987; Kurtz et al., 2000). This eliminates the need to understand the volume loss of the profile, to accurately quantify the mass loss (Chadwick et al., 1990; Hayes et al., 2019).

$$\Delta X_{Ti} = \frac{([X]_n/[Ti]_n - [X]_i/[Ti]_i)}{[X]_i/[Ti]_i} \quad (5)$$

Where X is the mobile element of interest, [Ti] is the titanium concentration, and *n* refers to a sample above the deepest or least weathered in the profile, and *i* identifies the deepest sample.

293 This loss quantity can be considered a “pseudo” tau value, as it is not trying to explicitly say
294 what the parent is, but rather quantifying a relative loss compared to the least weathered sample
295 (Anderson et al., 2002). Note, in our sample set we do not have the major elements for the
296 deepest Woodford sample, instead we use the next deepest sample to normalize these
297 calculations.

298 **3. Results:**

299 All raw sample data are found in the Supplementary Information (SI Table 1) and a complied
300 list of new measurements are in Table 1. First, we examined individual weathering profiles as
301 done previously in Jaffe et al. (2002) and Dalai et al. (2002), to examine the relationship between
302 Re geochemistry and OC_{petro} loss at the site scale. For example, in the New Albany Clay City
303 black shale weathering profile we find: i) an apparent coupled loss of OC_{petro} and Re with depth;
304 and ii) a deeper pyrite weathering front, suggesting sulfur depletion is spatially decoupled from
305 Re depletion (Figure 1). In this example, the unweathered samples had OC_{petro} concentrations of
306 ~7 to 8% and [Re] ~ 100 ng/g. In the weathered samples, OC_{petro} drops to 1.8% and [Re] drops to
307 1.52 ng/g, while sulfur is fully removed from the profile except for the most unweathered
308 sample. Similar patterns are observed in other new black shale and grey shale data and have been
309 observed in other weathering profiles (Hilton et al., 2021; Zhang et al., 2024).

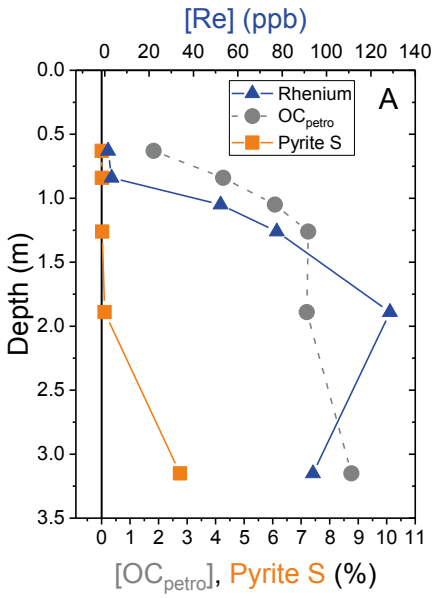

Figure 1: Example of rhenium and rock organic carbon (OC_{petro}) loss during weathering. A weathering profile from New Albany Clay City showing changes in OC_{petro}, pyrite S and rhenium concentration with depth in profile.

Other trace and major elements for each of the newly measured black shales are given in the SI Table 1. Concentrations of Ti are used to calculate the loss metric of [Re], [OC_{petro}], and a subset of mobile elements of interest such as Na, Ca, and S as described above (ΔX_{Ti}). The loss of Re does not correlate with any major element linked to carbonate weathering or silicate weathering (Figure 2A and B), and is not coupled with sulfide oxidation and iron cycling (Figure 2C and D). In more detail, we found that normalized Re loss ($\Delta[Re]_{Ti}$) was not significantly correlated (Pearson correlation) with calcium loss ($r = -0.10$, $p = 0.59$), sodium loss ($r = 0.09$, $p = 0.61$), sulfur loss ($r = -0.02$, $p = 0.93$); or iron loss ($r = 0.17$, $p = 0.40$).

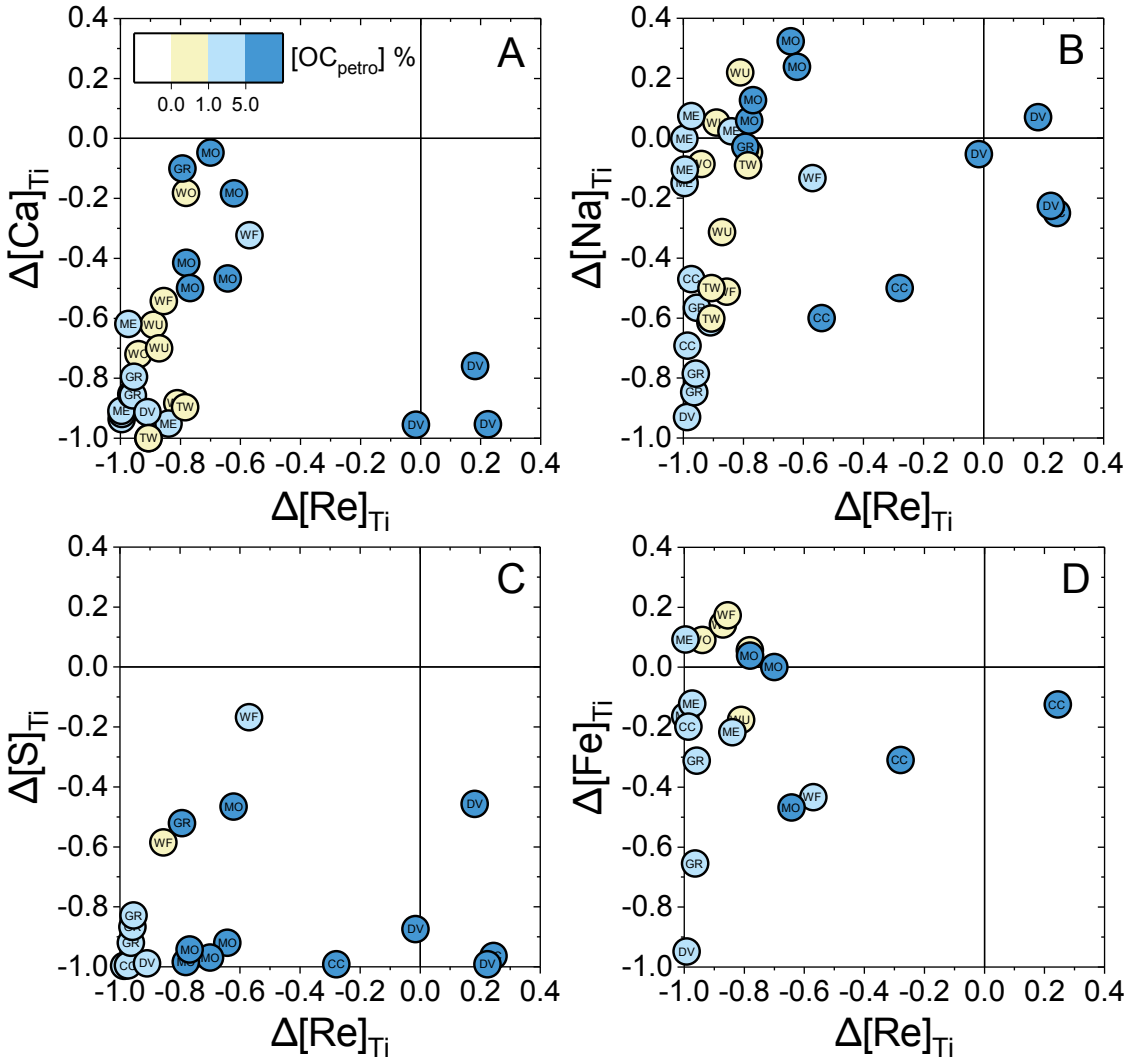

Figure 2: Relative changes in rhenium concentration in the studied weathering profiles, reported as a loss coefficient relative to the deepest sample and normalized to titanium concentrations. Rhenium loss plotted with: A: calcium loss (r = -0.10, p= 0.59); B: sodium loss (r = 0.09, p= 0.61); C: sulfur loss (r= -0.02 ,p=0.93); and D: iron loss (r =0.17 , p=0.40).

Across the weathering profiles, we found a significant correlation between OC_{petro} loss and Re loss ($r = 0.66$, $p < 0.05$). The average ratio of OC_{petro} and Re loss was 0.84 ± 0.15, with 8 out of 9 sites having a ratio >0.74. At one site (Marcellus Shale), the average ratio was lower at 0.58 ± 0.11 (Table 3), possibly due to the different thermal maturity of this shale (Dickson et al., 2020).

Table 3. List of shale weathering profiles and their respective average $\Delta[OC_{petro}]_{Ti}/\Delta[Re]_{Ti}$ loss ratio across measured samples, reported with the standard deviation.

Location	Rock type	$\Delta[OC_{petro}]_{Ti}/\Delta[Re]_{Ti}$
Waiapoa	gray shale	0.94± 0.05
Waipu	gray shale	0.78± 0.14
Marcellus	black shale	0.58± 0.12
New Albany (Clay city)	black shale	0.81± 0.15
Woodford Shale	black shale	0.74± 0.36
Green River	black shale	0.88± 0.18
Monterey	black shale	0.79± 0.18
Taiwan	grey shale	0.95± 0.09
East River	grey shale	1.11± 0.00
All sites	n.a.	0.84± 0.15

For the seven black shale weathering profiles, with an initial OC_{petro} content of 6.11–22.55 wt%, we assume the total OC in the shale is OC_{petro}. The weathered black shales range in OC content between 0.98–5.01 %. [Re] ranged from 31 ng/g to 671 ng/g in the un-weathered shale, and ranged from 0.38 ng/g to 278 ng/g in the weathered shales.

From the grey shale profiles from New Zealand, Taiwan, and the East River, OC_{petro} contents were expectedly much lower than in the black shales, as expected, with the least weathered samples having concentrations which range from 0.17 to 0.76%. Weathered materials have OC_{petro} contents of 0.04–0.38%. The [Re] of these grey shales is similarly low, ranging from 0.03–2.10 ng/g in the weathered samples and from 0.31–4.31 ng/g in the less weathered materials. These are more similar to the continental crustal value of < 1 ng/g (Peucker-Ehrenbrink and Jahn, 2001) than the concentrated Re values in the black shales.

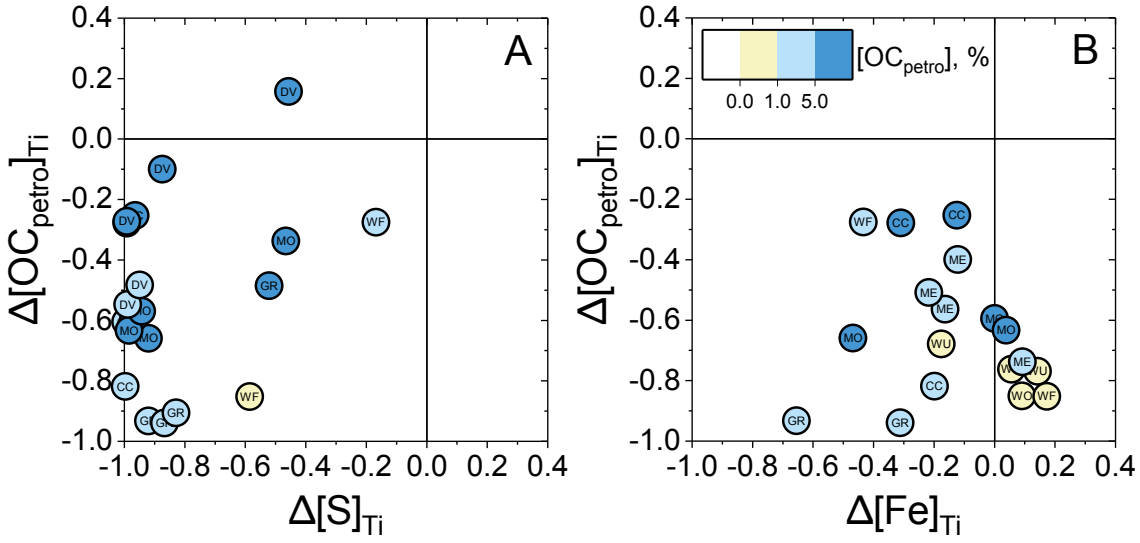

Figure 3: Relative changes in sulfur (S) and iron (Fe) in the studied weathering profiles. Differences between the concentrations of the deepest sample reported as a loss coefficient normalized to titanium concentrations, where negative values indicate relative loss and positive values indicate relative gain, for: A: rock organic carbon concentration (OC_{petro}) vs sulfur ; B: rock organic carbon concentration (OC_{petro}) vs iron.

Finally, we compared the OC_{petro} loss ($\Delta[OC_{petro}]_{Ti}$) to both the sulfur loss ($\Delta[S]_{Ti}$) and iron loss ($\Delta[Fe]_{Ti}$) across the measured profiles. We find that ($\Delta[OC_{petro}]_{Ti}$) does not correlate with ($\Delta[S]_{Ti}$), using a Pearson correlation ($r = 0.32$, $p = 0.16$) or $\Delta[Fe]_{Ti}$) ($r = 0.05$, $p = 0.81$). Sulfur and iron in these samples are likely coming from the initial oxidation of sulfides and then incorporated into secondary minerals and biogeochemical cycling. These results show OC_{petro} loss is decoupled from both sulfur and iron loss.

4. Discussion:

A number of studies have used isolated weathering profiles (e.g. Figure 1) to show that Re loss during weathering is coupled to OC_{petro} loss (Jaffe et al., 2002; Zhang et al., 2024), a key foundation in the use of the Re-proxy for OC_{petro} oxidation (Dalai et al., 2002). Here, we provide a systematic assessment of Re mobility, using immobile elements to robustly quantify element

losses across ranges in sedimentary rock types, OC_{petro} contents, and weathering intensities. We show that despite differences in climate, denudation rate, and tectonic setting, OC_{petro} loss and Re loss are linked in weathering profiles. This result confirms the appropriate use of the Re proxy in eq.1 for OC_{petro} oxidation studies.

4.1. Decoupling of Re loss from carbonate, silicate and sulfide weathering

Rhenium concentrations vary significantly between the different outcrops studied here (Table 1). This may reflect different hosts of Re in the solid phase, which are known to include OC_{petro} (Selby and Creaser, 2003), silicate minerals (Burton et al., 2002) and sulfides (Colodner et al., 1993; Dalai et al., 2002; Ross and Bustin, 2009). Carbonates are not thought to be a major host of Re (Miller et al., 2011), although diagenetic processes may redistribute Re and this has not been well studied (Helz, 2022). Generally, in silicate minerals, Re is thought to be relatively low concentration, as crustal abundances are on average of ~0.93 ng g^{-1} and 0.2–2 ng g^{-1} in oceanic and continental crust, respectively (Peucker-Ehrenbrink and Jahn, 2001).

Silicate weathering is generally measured through the flux of Na, Ca, Mg phases in river waters and weathered products, as the major rock types are composed of these base cations (Gaillardet et al., 1999). Carbonate weathering is tracked by the major elements Ca and Mg (Beaulieu et al., 2011; Spence and Telmer, 2005). Across the weathering profiles studied here, we find a correlation between Mg loss and Na loss (Pearson $r = 0.45$, $p = 0.0071$) and Mg loss and Ca loss ($r = 0.29$ value and $p = 0.12$, not significant). These patterns are broadly consistent with silicate and carbonate weathering processes operating across the sampling locations. Variability in these loss ratios will reflect the variability in the mineralogy of silicate and carbonate minerals, and the detailed reaction kinetics operating as a function of water residence

time and physical weathering processes (Brantley et al., 2013; Brantley et al., 2017; Gu et al., 2020), but is not the focus of the study here.

When we compare Re loss (ΔRe_{Ti}) to the tracers of silicate and carbonate weathering, we do not find any significant correlations (Figure 2). First, this suggests that across the profiles, silicate and carbonate minerals are not the dominant hosts of Re. This fits with findings from sequential extractions of Mackenzie River sediments, a mix of sedimentary rock grains, where only 3–7% of Re could be linked to a silicate-mineral host, and only <6% in a potential carbonate hosted pool (Dellinger et al., 2021). Similar sequential extractions results were reported in Zhang et al. (2024). Miller et al. (2015), also suggested silicates and carbonate are a minor host of Re using Re isotope mass balance. Second, it suggests that the bulk loss of Re is not being meaningfully driven by silicate or carbonate mineral weathering.

Sulfides have been proposed as a potential host of Re in sedimentary rocks and an important source of Re in global rivers, based on a broad and scattered relationship between dissolved Re and SO_4^{2-} concentrations (Miller et al., 2011). However, this has been disputed by dissolved ion mixing analyses in the Mackenzie River and Rio Madre de Dios (Dellinger et al., 2023; Horan et al., 2019), which point toward sulfide minerals only being a dominant host of Re in a handful of small catchments. Hydrological behavior of Re in alpine streams also appears to be decoupled from the production and export of SO_4^{2-}, a weathering product of sulfide oxidation (Hilton et al., 2021; Winnick et al., 2017). Indeed, in support of these river-based studies, we find that individual weathering profiles show a decoupling of S loss and Re loss (Figure 1) similar to the first assessment of Re loss across a black shale weathering profile (Jaffe et al., 2002). Overall, across the black and grey shales studied here, we find no meaningful relationship between S loss (i.e. sulfide oxidation) and Re loss (Figure 2C). While this does not preclude

396 sulfides as an important Re host in some locations, it suggests that Re loss and delivery to the
397 hydrosphere and river waters is not closely coupled to sulfide oxidation.
398
399 **4.2. Coupled loss of Re and OC_{petro} across weathering profiles**
400 We find a systematic loss of Re and OC_{petro} across the black and grey shale weathering profiles
401 (Figure 3) and the ΔRe_{Ti} and $\Delta[OC_{petro}]_{Ti}$ values are statistically significant ($r = 0.66$, $p < 0.05$).
402 About 17 samples lie within ±10% of congruent, 1:1 Re and OC_{petro} loss during weathering. This
403 occurs in samples with variable Re and OC_{petro} concentrations, initial Re to OC_{petro} ratios in rocks
404 (Table 3), relative losses of Re and S (Figure 2C,D), and variations in Fe cycling (Figure 4).
405 Additionally, our sample set ranges in weathering intensity, climatic and geomorphic settings,
406 different physical rock properties, and different geochemical characteristics of OC_{petro}. The first
407 order conclusion from these findings is that Re provides a robust proxy for OC_{petro} oxidation.

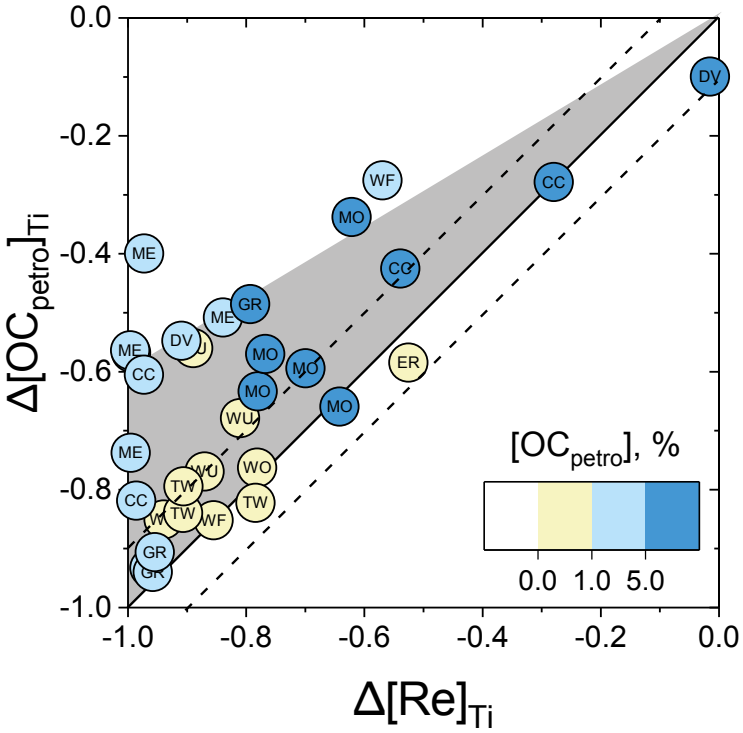

Figure 4: OC_{petro} and Re loss in the weathering profiles, accounting for volume changes using Ti normalization. A 1:1 loss ratio is shown as a black line. Dashed lines indicate a 1:1 loss to within ±10%. The shaded grey domain is the predicted region (Equation 4) based on the combination of: i) presence of Re hosted in sulfide and silicate phases alongside OC_{petro}, and ii) incomplete weathering of OC_{petro}.

In more detail, we find that the average ratio of $\Delta[OC_{petro}]_{Ti}$ to ΔRe_{Ti} is 0.84± 0.15, and several sites have values < 1. There are three reasons why Re loss may be proportionally more than OC_{petro} loss which have been discussed in the literature (Horan et al., 2019). First, while Re loss is not clearly linked to carbonate, silicate, and sulfide weathering patterns (Figure 2), these phases could host >10% of the Re within some rock types. The contributions of Re from organic matter vs carbonate, silicate and sulfide phases could vary based on depositional setting, and geochemistry of the initial sedimentation environment and the continued diagenesis of the sediments (Sheen et al., 2018) and inorganic weathering of Re can proceed without OC

417 oxidation. Second, Re is a highly mobile, soluble element (Colodner et al., 1993) in oxic
418 environments whose association with organic matter in rocks is still not well understood (Selby
419 and Creaser, 2003). It is possible that Re may be mobilized during water-rock interactions while
420 some OC_{petro} is not lost. Finally, OC_{petro} may include physically protected organic matter (Gu and
421 Brantley, 2022) or thermally mature OC_{petro}, including graphite, which is more resistant to
422 OC_{petro} oxidation and that may or may not host Re (Toma et al., 2022). The presence of more
423 recalcitrant OC could lead to a residue of unweathered, Re-poor OC_{petro} accumulating in soils
424 and weathered rocks.
425 There is relatively little known about the detailed chemical association of Re and OC_{petro}.
426 We know that during reduction in surface marine sediments where OC accumulates, ReO_4^- is
427 immobilized (Colodner et al., 1993; Crusius and Thomson, 2000). Inorganic thermodynamic
428 considerations predict that rhenium may be precipitated as ReS_2 (Chappaz et al., 2008;
429 Yamashita et al., 2007), or form thioperrhenate ($ReOxS4-x^-$) or Re(VII)-sulfide precipitates
430 (Helz and Dolor, 2012; Vorlicek et al., 2015). A co-precipitation of iron-based phases has also
431 been invoked in sulfidic waters (Helz, 2022; Helz and Dolor, 2012). However, correlations
432 between OC and Re in sedimentary rocks, chemical extractions of Re from shales (Selby and
433 Creaser, 2003) support a dominant role of an organic matter host, also indirectly supported by
434 the observed coupled loss of Re and OC (Figure 3).
435 Regardless of the details of the organic matter host for Re, it is plausible that there are a
436 range of OC_{petro}-S-Re bonding environments that form in many sedimentary rocks. These could
437 have different weathering rates based on their inherent or apparent reactivity. For instance, the
438 majority Re could be hosted in a “fast weathering” OC_{petro} structure that is linked to an early
439 diagenetic process of reduction in marine sediments. In contrast, Re-poor organic matter

delivered from terrestrial ecosystems may be mineral-bound (Repasch et al., 2021), and this may weather at a different rate. The weathering profile with the lowest $\Delta[OC_{petro}]_{Ti}$ to ΔRe_{Ti} ratio is the Marcellus shale which is known to be more thermally mature than the other black shales in this study. In summary, it is unlikely that all OC_{petro} is homogenous, meaning OC_{petro} and associated Fe and S phases could weather incongruently, which may have variable Re concentrations depending on depositional environment, mixing, and subsequent diagenesis.

An addition consideration is that the OC_{petro} and Re might have different bioavailability, which could lead to a discrepancy in the measured loss ratio. The bioavailability of Re in terrestrial or marine systems is not well understood, with very few studies measuring Re in plant or microbial tissues (Ghazi et al., 2024). While Re has no known role in biology and is not an essential trace element for biological function in either the terrestrial or marine systems, some uptake has been observed in corals of the gulf coast (Prouty et al., 2014), but has not been widely measured in other plant tissues. However, OC_{petro} may be utilized by microbial life, as carbon sources are important for microbial and plant life. Petsch et al. (2001) found uptake of ^{14}C free organic matter into the microbial cell walls of living biomass, while Hemingway et al. (2018) measured OC_{petro} oxidation in Taiwan of up to 60%, meaning that a large portion of OC could be mineralized and potentially utilized for microbial metabolism. This potentially could lead to a discrepancy in the 1:1 Re/OC_{petro} if OC_{petro} is preferentially removed from the system, while Re is conservative.

In most profiles, we find Re loss relative to the least weathered sample. However, there are a few samples which show elevated Re concentrations and an apparent Re enrichment. Based on our current understanding of the Re system, there are two explanations for these elevated Re concentrations. The first is an anthropogenic input of Re. The sampled road cuts are not entirely

463 isolated from wet or dry atmospheric deposition, either onto the surface of the outcrop, or from
464 the surface soil down via critical zone processes such as root invasion, water percolation, and
465 freeze/thaw cycles. In the northeast USA, where the NACC and NADV samples were collected,
466 Ogrič et al. (2023) found elevated anthropogenic Re input to the upper few centimeters of soils
467 in the Shale Hills CZO likely due to coal burning and local industry. In that small catchment, the
468 majority of the dissolved Re in streams was derived from anthropogenic inputs rather than
469 weathering (Ogric et al., 2023). It is thus reasonable that some atmospheric deposition of Re
470 could have occurred at some sites. The Re to OC_{petro} ratio of this material is not well constrained,
471 but may differ from that in bulk sedimentary rocks. Another possibility discussed by Jaffe et al.
472 (2002), is that Re could be transported vertically through the soil. These profiles are above
473 ground and are likely influenced by organic acids and precipitation transported through the
474 soil/regolith system. Soils undergo microscale redox processes, so under certain conditions, there
475 could be Re mobilization and movement in the subsurface, but not complete loss to the river
476 system. This could cause elevated [Re] based on the critical zone properties.
477

478 Despite these caveats, we find the range of $\Delta[OC_{petro}]_{Ti}$ to ΔRe_{Ti} values that have been used in

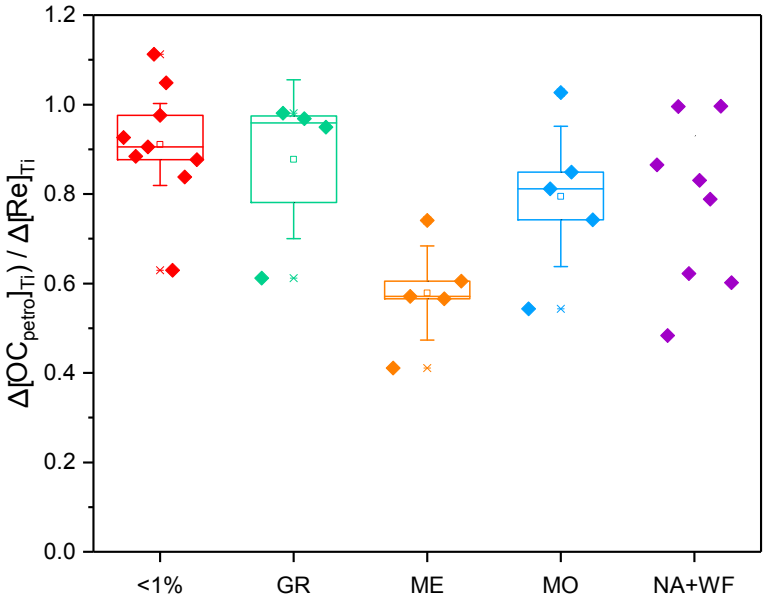

Figure 5: Ratio of titanium normalized loss relative to the deepest sample in each profile (Figure 4), with box showing the interquartile range, line showing the median, square showing the mean, and whiskers showing the 2SE bounds. The sites are sub-grouped for profiles with <1% OC_{petro} (WPO, WPU, ER, TW), GR (Green River), ME (Marcellus Shale), MO (Monterey Shale) and a subgroup of the New Albany and Woodford Shales (NACC, NADV, WF).

479 studies using dissolved Re proxy to calculate OC_{petro} oxidation are robust. These are shown by
480 the shaded part of Figure 4, using typical ranges of $f_C + f_{graphite}$ values (assumed to be ~0-30%)
481 (Equation 1). The fact that all the weathered materials sit within this domain provides further
482 support for the proxy. We find that the absolute ratio of Re loss to OC_{petro} loss (without Ti
483 normalization) is rather consistent for grey shales, with a value of $2.7 \pm 1.6 \times 10^{-7}$ g g^{-1} (SI Table
484 1). This is similar to values used in a recent global analysis of river Re fluxes and application of
485 the Re proxy (Zondervan et al., 2023), suggesting no systematic bias in these fluxes. However,
486 the absolute ratio of Re and OC_{petro} loss (without Ti normalization) does differ across the profiles

studied here in the black shales (SI Table 1) ranging from 1.16 x 10^{-8} g g^{-1} to 5.56 x 10^{-6} g g^{-1} with the average being 1.2 ± 1.6 x 10^{-6} g g^{-1} (SI Table 1) about an order of magnitude more than the grey shales, showing how important it can be at a small catchment-scale to try and constrain the behavior of Re and OC_{petro} in the weathering zone using an index element normalization.

Finally, we note that by studying the weathering residues, we cannot conclude the fate of the lost OC_{petro} (Petsch, 2014). While Re is likely to be oxidized to the soluble ion ReO_4^-, OC_{petro} could be oxidized to CO_2, as measured in exposed mudstones of New Zealand (Roylands et al., 2022) and marls of the French pre-Alps (Soulet et al., 2021), along with deep sedimentary tills (Keller and Bacon, 1998) and mudstones in the Eel River catchment (Tune et al., 2020). Alternatively, the microbial-processing of OC_{petro} (Matlakowska and Sklodowska, 2011; Wlodarczyk et al., 2018) could lead to biomass build up in the weathered rocks that may be ^{14}C-depleted (Hemingway et al., 2018; Petsch et al., 2001a) and/or be leached as dissolved organic matter away from the weathering site (Schillawski and Petsch, 2008). This microbial biomass or dissolved organic matter may then be bioavailable for heterotrophic consumption (Schillawski and Petsch, 2008). Therefore, while the study here concludes the loss of Re is a robust proxy for OC_{petro} loss during weathering, and likely CO_2 production, a coupled approach which seeks to track carbon species at a variety of scales alongside trace metal and Re mobility will provide further insight to how OC_{petro} weathering impacts the geochemical carbon cycle.

5. Conclusions

To appropriately quantify OC_{petro} weathering fluxes, the Re proxy must be validated. This study clearly shows that across a range of weathering rates, scales, denudation rates, geochemical content, the Re proxy for OC_{petro} oxidation is robust. OC_{petro} weathering contributes to an equal

flux that is drawn down by silicate weathering, thus it is an important, but understudied part of the global carbon cycle. We find a broad correlation between OC_{petro} and Re across our samples, with no correlation between Re and products of sulfide, carbonate, or silicate weathering. While we cannot rule out some influence in the Re flux from these other sources, our finding suggest that OC_{petro} is the dominate host of Re. We find the average value of 0.84 ±0.15 for the loss ratio of OC_{petro} and Re ($\Delta[OCpetro]_{Ti}/\Delta[Re]_{Ti}$) across gray and black shales of different chemistries and we urge this value to be used in systems as an estimate of the (1- ($f_c + f_{graphite}$)) *term* in the calculation of OCpetro oxidation from dissolved Re flux (Equation 1). The [Re] proxy for calculating OC_{petro} fluxes across environments is valid and can be used to constrain OC_{petro} input to modern environments.

6. Acknowledgements

This research was funded by an European Research Council (ERC) Starting Grant to RGH, ROC-CO_2 project, grant 678779 and by a Natural Environment Research Council (NERC) grant to RGH, AD and MD (NE/T001119). Partial writing of this work was performed under the auspices of the U.S. Department of Energy by Lawrence Livermore National Laboratory under Contract DE-AC52-07NA27344 and was supported by the LLNL LDRD Program under Project No. 24-LW-049. LLNL-JRNL-2000144.

7. Works Cited

1. Anderson, S.P., Dietrich, W.E., Brimhall, G.H., Jr., 2002. Weathering profiles, mass-balance analysis, and rates of solute loss: Linkages between weathering and erosion in a small, steep catchment. GSA Bulletin, 114(9): 1143-1158.

2. Beaulieu, E. et al., 2011. Modeling of water-rock interaction in the Mackenzie basin: Competition between sulfuric and carbonic acids. Chemical Geology, 289(1): 114-123.

3. Beck, H. E., T. R. McVicar, N. Vergopolan, A. Berg, N. J. Lutsko, A. Dufour, Z. Zeng, X. Jiang, A. I. J. M. van Dijk, and D. G. Miralles (2023), High-resolution (1 km) Köppen-Geiger maps for 1901–2099 based on constrained CMIP6 projections, *Scientific Data*, *10*(1), 724, doi:10.1038/s41597-023-02549-6.

4. Berner, R.A., 2003. The long-term carbon cycle, fossil fuels and atmospheric composition. Nature, 426(6964): 323-326.

5. Blair, N.E. et al., 2003. The persistence of memory: the fate of ancient sedimentary organic carbon in a modern sedimentary system. Geochimica et Cosmochimica Acta, 67(1): 63-73.

6. Bolton, E.W., Berner, R.A., Petsch, S.T., 2006. The weathering of sedimentary organic matter as a control on atmospheric O2: II. Theoretical modeling. American Journal of Science, 306(8): 575-615.

7. Brantley, S.L., Holleran, M.E., Jin, L., Bazilevskaya, E., 2013. Probing deep weathering in the Shale Hills Critical Zone Observatory, Pennsylvania (USA): the hypothesis of nested chemical reaction fronts in the subsurface. Earth Surface Processes and Landforms, 38(11): 1280-1298.

8. Brantley, S.L. et al., 2017. Toward a conceptual model relating chemical reaction fronts to water flow paths in hills. Geomorphology, 277: 100-117.

9. Brimhall, G.H., Dietrich, W.E., 1987. Constitutive mass balance relations between chemical composition, volume, density, porosity, and strain in metasomatic hydrochemical systems: Results on weathering and pedogenesis. Geochimica et Cosmochimica Acta, 51(3): 567-587.

10. Burton, K.W. et al., 2002. The compatibility of rhenium and osmium in natural olivine and their behaviour during mantle melting and basalt genesis. Earth and Planetary Science Letters, 198(1): 63-76.

11. Chadwick, O.A., Brimhall, G.H., Hendricks, D.M., 1990. From a black to a gray box — a mass balance interpretation of pedogenesis. Geomorphology, 3(3): 369-390.

12. Chappaz, A., Gobeil, C., Tessier, A., 2008. Sequestration mechanisms and anthropogenic inputs of rhenium in sediments from Eastern Canada lakes. Geochimica et Cosmochimica Acta, 72(24): 6027-6036.

13. Colodner, D. et al., 1993. The geochemical cycle of rhenium: a reconnaissance. Earth and Planetary Science Letters, 117(1): 205-221.

14. Copard, Y., Amiotte-Suchet, P., Di-Giovanni, C., 2007. Storage and release of fossil organic carbon related to weathering of sedimentary rocks. Earth and Planetary Science Letters, 258(1-2): 345-357.

15. Crusius, J., Thomson, J., 2000. Comparative behavior of authigenic Re, U, and Mo during reoxidation and subsequent long-term burial in marine sediments. Geochimica et Cosmochimica Acta, 64(13): 2233-2242.

16. Cumming, V.M., Poulton, S.W., Rooney, A.D., Selby, D., 2013. Anoxia in the terrestrial environment during the late Mesoproterozoic. Geology, 41(5): 583-586.

17. Dalai, T.K., Singh, S.K., Trivedi, J.R., Krishnaswami, S., 2002. Dissolved rhenium in the Yamuna river system and the Ganga in the Himalaya: role of black shale weathering on the budgets of Re, Os, and U in rivers and CO2 in the atmosphere. Geochimica et Cosmochimica Acta, 66(1): 29-43.

18. Dellinger, M. et al., 2023. High rates of rock organic carbon oxidation sustained as Andean sediment transits the Amazon foreland-floodplain. Proceedings of the National Academy of Sciences, 120(39): e2306343120.

19. Dellinger, M., Hilton, R.G., Nowell, G.M., 2020. Measurements of rhenium isotopic composition in low-abundance samples. Journal of Analytical Atomic Spectrometry, 35(2): 377-387.

20. Dellinger, M., Hilton, R.G., Nowell, G.M., 2021. Fractionation of rhenium isotopes in the Mackenzie River basin during oxidative weathering. Earth and Planetary Science Letters, 573.

21. Dickson, A.J., Idiz, E., Porcelli, D., van den Boorn, S.H.J.M., 2020. The influence of thermal maturity on the stable isotope compositions and concentrations of molybdenum, zinc and cadmium in organic-rich marine mudrocks. Geochimica et Cosmochimica Acta, 287: 205-220.

22. Gaillardet, J., Dupré, B., Louvat, P., Allègre, C.J., 1999. Global silicate weathering and CO2 consumption rates deduced from the chemistry of large rivers. Chemical Geology, 159(1): 3-30.

23. Galy, V., Beyssac, O., France-Lanord, C., Eglinton, T., 2008. Recycling of Graphite During Himalayan Erosion: A Geological Stabilization of Carbon in the Crust. Science, 322(5903): 943-945.

24. Galy, V., Bouchez, J., France-Lanord, C., 2007. Determination of Total Organic Carbon Content and δ13C in Carbonate-Rich Detrital Sediments. Geostandards and Geoanalytical Research, 31(3): 199-207.

25. Ghazi, L., Goñi, M., Haley, B.A., Muratli, J.M., Pett-Ridge, J.C., 2022. Concentration-runoff relationships of contrasting small mountainous rivers in the Pacific Northwest, USA: Insights into the weathering of rhenium relative to other weathering products. Geochimica et Cosmochimica Acta, 337: 106-122.

26. Ghazi, L., K. E. Grant, A. Chappaz, M. Danish, B. Peucker-Ehrenbrink, and J. C. Pett-Ridge (2024), The Global Biogeochemical Cycle of Rhenium, *Global Biogeochemical Cycles*, *38*(10), doi:10.1029/2024gb008254.

27. Gu, X., Brantley, S.L., 2022. How particle size influences oxidation of ancient organic matter during weathering of black shale. ACS Earth and Space Chemistry, 6(6): 1443-1459.

28. Gu, X. et al., 2020. Chemical reactions, porosity, and microfracturing in shale during weathering: The effect of erosion rate. Geochimica et Cosmochimica Acta, 269: 63-100.

29. Hayes, J.L., Riebe, C.S., Holbrook, W.S., Flinchum, B.A., Hartsough, P.C., 2019. Porosity production in weathered rock: Where volumetric strain dominates over chemical mass loss. Science Advances, 5(9): eaao0834.

30. Helz, G.R., 2022. The Re/Mo redox proxy reconsidered. Geochimica et Cosmochimica Acta, 317: 507-522.

31. Helz, G.R., Dolor, M.K., 2012. What regulates rhenium deposition in euxinic basins? Chemical Geology, 304: 131-141.

32. Hemingway, J.D. et al., 2018. Microbial oxidation of lithospheric organic carbon in rapidly eroding tropical mountain soils. Science, 360(6385): 209-212.

33. Hilton, R.G., Gaillardet, J., Calmels, D., Birck, J.-L., 2014. Geological respiration of a mountain belt revealed by the trace element rhenium. Earth and Planetary Science Letters, 403: 27-36.

34. Hilton, R.G., Galy, A., Hovius, N., Horng, M.-J., Chen, H., 2010. The isotopic composition of particulate organic carbon in mountain rivers of Taiwan. Geochimica et Cosmochimica Acta, 74(11): 3164-3181.

35. Hilton, R.G., Galy, A., Hovius, N., Horng, M.-J., Chen, H., 2011. Efficient transport of fossil organic carbon to the ocean by steep mountain rivers: An orogenic carbon sequestration mechanism. Geology, 39(1): 71-74.

36. Hilton, R.G. et al., 2021. Concentration-Discharge Relationships of Dissolved Rhenium in Alpine Catchments Reveal Its Use as a Tracer of Oxidative Weathering. Water Resources Research, 57(11): e2021WR029844.

37. Hilton, R.G., West, A.J., 2020. Mountains, erosion and the carbon cycle. Nature Reviews Earth & Environment, 1(6): 284-299.

38. Horan, K. et al., 2019. Carbon dioxide emissions by rock organic carbon oxidation and the net geochemical carbon budget of the Mackenzie River Basin. American Journal of Science, 319(6): 473-499.

39. Horan, K. et al., 2017. Mountain glaciation drives rapid oxidation of rock-bound organic carbon. Sci Adv, 3(10): e1701107.

40. Jaffe, L.A., Peucker-Ehrenbrink, B., Petsch, S.T., 2002. Mobility of rhenium, platinum group elements and organic carbon during black shale weathering. Earth and Planetary Science Letters, 198(3): 339-353.

41. Keller, C.K., Bacon, D.H., 1998. Soil respiration and georespiration distinguished by transport analyses of vadose CO2, 13CO2, and 14CO2. Global Biogeochemical Cycles, 12(2): 361-372.

42. Komada, T., M. R. Anderson, and C. L. Dorfmeier (2008), Carbonate removal from coastal sediments for the determination of organic carbon and its isotopic signatures, δ13C and Δ14C: comparison of fumigation and direct acidification by hydrochloric acid, *Limnology and Oceanography: Methods*, *6*(6), 254-262, doi:10.4319/lom.2008.6.254.

43. Kuehl, S.A. et al., 2016. A source-to-sink perspective of the Waipaoa River margin. Earth-Science Reviews, 153: 301-334.

44. Kurtz, A.C., Derry, L.A., Chadwick, O.A., Alfano, M.J., 2000. Refractory element mobility in volcanic soils. Geology, 28(8): 683-686.

45. Matlakowska, R., Sklodowska, A., 2011. Biodegradation of Kupferschiefer black shale organic matter (Fore-Sudetic Monocline, Poland) by indigenous microorganisms. Chemosphere, 83(9): 1255-1261.

46. Mazengarb, C., I.G.Speden, 2000. Geology of the Raukumara Area, vol. 6. Institute of Geological & Nuclear Sciences 1:250 000 geological map.

47. McIntyre, C. P., L. Wacker, N. Haghipour, T. M. Blattmann, S. Fahrni, M. Usman, T. I. Eglinton, and H.-A. Synal (2017), Online 13C and 14C Gas Measurements by EA-IRMS–AMS at ETH Zürich, *Radiocarbon*, *59*(3), 893-903, doi:10.1017/RDC.2016.68.

48. Miller, C.A., Peucker-Ehrenbrink, B., Schauble, E.A., 2015. Theoretical modeling of rhenium isotope fractionation, natural variations across a black shale weathering profile, and potential as a paleoredox proxy. Earth and Planetary Science Letters, 430: 339-348.

49. Miller, C.A., Peucker-Ehrenbrink, B., Walker, B.D., Marcantonio, F., 2011. Re-assessing the surface cycling of molybdenum and rhenium. Geochimica et Cosmochimica Acta, 75(22): 7146-7179.

50. Ogrič, M. et al., 2023. Low rates of rock organic carbon oxidation and anthropogenic cycling of rhenium in a slowly denuding landscape. Earth Surface Processes and Landforms, n/a(n/a): 1202-1218.

51. Petsch, S., Eglinton, T., Edwards, K., 2001a. 14C-dead living biomass: evidence for microbial assimilation of ancient organic carbon during shale weathering. science, 292(5519): 1127-1131.

52. Petsch, S.T., 2014. 12.8 - Weathering of Organic Carbon. In: Holland, H.D., Turekian, K.K. (Eds.), Treatise on Geochemistry (Second Edition). Elsevier, Oxford, pp. 217-238.

53. Petsch, S.T., Berner, R.A., Eglinton, T.I., 2000. A field study of the chemical weathering of ancient sedimentary organic matter. Organic Geochemistry, 31(5): 475-487.

54. Petsch, S.T., Smernik, R.J., Eglinton, T.I., Oades, J.M., 2001b. A solid state 13C-NMR study of kerogen degradation during black shale weathering. Geochimica et Cosmochimica Acta, 65(12): 1867-1882.

55. Peucker-Ehrenbrink, B., Hannigan, R.E., 2000. Effects of black shale weathering on the mobility of rhenium and platinum group elements. Geology, 28(5): 475-478.

56. Peucker-Ehrenbrink, B., Jahn, B.-m., 2001. Rhenium-osmium isotope systematics and platinum group element concentrations: Loess and the upper continental crust. Geochemistry, Geophysics, Geosystems, 2(10): n/a-n/a.

57. Prouty, N. G., E. B. Roark, A. E. Koenig, A. W. J. Demopoulos, F. C. Batista, B. D. Kocar, D. Selby, M. D. McCarthy, F. Mienis, and S. W. Ross (2014), Deep-sea coral record of human impact on watershed quality in the Mississippi River Basin, Global Biogeochemical Cycles, 28(1), 29-43, doi:https://doi.org/10.1002/2013GB004754

58. Repasch, M. et al., 2021. Fluvial organic carbon cycling regulated by sediment transit time and mineral protection. Nature Geoscience, 14(11): 842-848.

59. Ross, D.J.K., Bustin, R.M., 2009. Investigating the use of sedimentary geochemical proxies for paleoenvironment interpretation of thermally mature organic-rich strata: Examples from the Devonian–Mississippian shales, Western Canadian Sedimentary Basin. Chemical Geology, 260(1): 1-19.

60. Roylands, T. et al., 2022. Capturing the short-term variability of carbon dioxide emissions from sedimentary rock weathering in a remote mountainous catchment, New Zealand. Chemical Geology, 608.

61. Roylands, T. et al., 2024. Probing the exchange of CO2 and O2 in the shallow critical zone during weathering of marl and black shale. Earth Surf. Dynam., 12(1): 271-299.

62. Salles, T. et al., 2023. Hundred million years of landscape dynamics from catchment to global scale. Science, 379(6635): 918-923.

63. Schillawski, S., Petsch, S., 2008. Release of biodegradable dissolved organic matter from ancient sedimentary rocks. Global Biogeochemical Cycles, 22(3): n/a-n/a.

64. Selby, D., Creaser, R.A., 2003. Re–Os geochronology of organic rich sediments: an evaluation of organic matter analysis methods. Chemical Geology, 200(3): 225-240.

65. Sheen, A.I. et al., 2018. A model for the oceanic mass balance of rhenium and implications for the extent of Proterozoic ocean anoxia. Geochimica et Cosmochimica Acta, 227: 75-95.

66. Soulet, G. et al., 2021. Temperature control on CO2 emissions from the weathering of sedimentary rocks. Nature Geoscience, 14(9): 665-671.

67. Spence, J., Telmer, K., 2005. The role of sulfur in chemical weathering and atmospheric CO2 fluxes: Evidence from major ions, δ13CDIC, and δ34SSO4 in rivers of the Canadian Cordillera. Geochimica et Cosmochimica Acta, 69(23): 5441-5458.

68. Stuiver, M., Polach, H.A., 1977. Discussion Reporting of 14C Data. Radiocarbon, 19(3): 355-363.

69. Syvitski, J.P., Kettner, A.J., Correggiari, A., Nelson, B.W., 2005. Distributary channels and their impact on sediment dispersal. Marine Geology, 222: 75-94.

70. Toma, J. et al., 2022. Re-Os systematics and chronology of graphite. Geochimica et Cosmochimica Acta, 323: 164-182.

71. Tune, A.K., Druhan, J.L., Wang, J., Bennett, P.C., Rempe, D.M., 2020. Carbon Dioxide Production in Bedrock Beneath Soils Substantially Contributes to Forest Carbon Cycling. Journal of Geophysical Research: Biogeosciences, 125(12).

72. Vorlicek, T.P., Chappaz, A., Groskreutz, L.M., Young, N., Lyons, T.W., 2015. A new analytical approach to determining Mo and Re speciation in sulfidic waters. Chemical Geology, 403: 52-57.

73. Wildman, R.A. et al., 2004. The weathering of sedimentary organic matter as a control on atmospheric O₂: I. Analysis of a black shale. American Journal of Science, 304(3): 234-249.

74. Winnick, M.J. et al., 2017. Snowmelt controls on concentration-discharge relationships and the balance of oxidative and acid-base weathering fluxes in an alpine catchment, East River, Colorado. Water Resources Research, 53(3): 2507-2523.

75. Wlodarczyk, A. et al., 2018. The Oxidative Metabolism of Fossil Hydrocarbons and Sulfide Minerals by the Lithobiontic Microbial Community Inhabiting Deep Subterrestrial Kupferschiefer Black Shale. Front Microbiol, 9: 972.

76. Yamashita, Y., Takahashi, Y., Haba, H., Enomoto, S., Shimizu, H., 2007. Comparison of reductive accumulation of Re and Os in seawater–sediment systems. Geochimica et Cosmochimica Acta, 71(14): 3458-3475.

77. Zhang, Y., J. Wang, Y. Qu, C. Zhu, and Z. Jin (2024), Mobility of rhenium and selenium during chemical weathering and their implication for petrogenic organic carbon oxidation, *Science China Earth Sciences*, *67*(3), 740-750, doi:10.1007/s11430-023-1244-5.

78. Zondervan, J.R. et al., 2023. Rock organic carbon oxidation CO2 release offsets silicate weathering sink. Nature.